

Article

Optoelectronic Properties of Ferroelectric Composites of $\text{Bi}_{3.25}\text{La}_{0.75}\text{Ti}_3\text{O}_{12}$ (BLT) and Co-Doped BLT Thin Films Modified by FeCo-Doped BLT

Rui Tang ^{1,†}, Rui He ^{1,†} , Sangmo Kim ^{2,*} and Chung Wung Bark ^{1,*} 

¹ Department of Electrical Engineering, Gachon University, Seongnam 13120, Republic of Korea; qq782366490@gmail.com (R.T.); herui6183@gmail.com (R.H.)

² Department of Intelligent Mechatronics Engineering, Sejong University, Seoul 05006, Republic of Korea

* Correspondence: sangmokim@sejong.ac.kr (S.K.); bark@gachon.ac.kr (C.W.B.)

† These authors contributed equally to this work.

Abstract: Driven by the growing demand for renewable and clean energy, the photovoltaic effect of various solar cells and materials was investigated for the conversion of light energy into electricity. We modified the $\text{Bi}_{3.25}\text{La}_{0.75}\text{Ti}_3\text{O}_{12}$ (BLT) and Co-doped BLT (Co-BLT) composites with Fe and Co-doped BLT (FeCo-BLT) films to narrow the bandgap and increase visible light absorption, thereby improving the efficiency of the photovoltaic reaction. In this study, BLT and Co-BLT thin films were fabricated by off-axis sputtering and then modified with FeCo-BLT thin films to produce dual-ferroelectric, thin-film composite materials that improved the photovoltaic power generation performance. Photoelectric test results showed that the modified double-ferroelectric, thin-film composites had superior optoelectronic properties. The current density was significantly enhanced by modifying the BLT films with doped Fe and Co. Therefore, this modification improved the efficiency of ferroelectric thin-film photovoltaic reactions.

Keywords: ferroelectric; thin film; photocurrent density; bandgap



Citation: Tang, R.; He, R.; Kim, S.; Bark, C.W. Optoelectronic Properties of Ferroelectric Composites of $\text{Bi}_{3.25}\text{La}_{0.75}\text{Ti}_3\text{O}_{12}$ (BLT) and Co-Doped BLT Thin Films Modified by FeCo-Doped BLT. *Coatings* **2023**, *13*, 1223. <https://doi.org/10.3390/coatings13071223>

Academic Editor: Amin Bahrami

Received: 5 June 2023

Revised: 26 June 2023

Accepted: 5 July 2023

Published: 8 July 2023



Copyright: © 2023 by the authors. Licensee MDPI, Basel, Switzerland. This article is an open access article distributed under the terms and conditions of the Creative Commons Attribution (CC BY) license (<https://creativecommons.org/licenses/by/4.0/>).

1. Introduction

Solar energy is a renewable source of energy that, owing to its wide range of distribution, has gradually replaced some nonrenewable energy resources, providing a reliable and effective way to solve the energy crisis. Photovoltaic power generation, one of the main uses of solar energy, is based on the principle that light irradiation of photosensitive materials results in a photoelectron transfer reaction that produces an electric potential difference at both ends of the material. Conventional solar cells are fabricated using p–n junctions, where the built-in electric field at the p–n junction interface spatially separates photogenerated carriers based on the junctions from which they are produced; for example, this interface separates the electrons produced by the p-junction from the holes produced by the n-junction. The separation of these carriers results in the generation of a photocurrent. [1–5]. Therefore, the photogenerated voltage of solar cells is limited by the size of the built-in electric field in the heterojunction. Although the photoelectric conversion efficiency of these cells is close to its maximum level, the photogenerated voltage does not satisfy the current demand. To develop low-cost and highly efficient photovoltaics, researchers are working towards developing new and improved photovoltaic materials.

Among photovoltaic materials, ferroelectric substances are highly regarded for their photovoltaic effect and theoretically high photoelectric conversion efficiency. The electric-field-modulated photovoltaic effect of ferroelectrics is not limited by the crystal forbidden bandwidth (E_g) as it can reach values of 10^3 – 10^5 V/cm, which is 2–4 orders of magnitude higher than that of E_g . The photovoltaic effect of ferroelectric materials differs from that of conventional p–n junction solar cells because these materials are excited by their unique

electric dipole [6–9]. The electric dipole feature of ferroelectrics, which is considered a “bulk effect”, can enhance the photoelectric conversion efficiency of solar cells [10,11].

$\text{Bi}_{3.25}\text{La}_{0.75}\text{Ti}_3\text{O}_{12}$ (BLT) is a typical lead-free ferroelectric thin film with a low forbidden bandwidth ($E_g = 2.2\text{--}2.7$ eV); it is known as a third-generation photocatalyst. Owing to its excellent ferroelectric properties, the endogenous electric field generated by the spontaneous polarization of BLT can accelerate charge transport and lead to energy band bending, which can effectively inhibit the compounding of photogenerated carriers. Therefore, it is often used to construct composite systems to improve the separation efficiency and photocurrent density of photogenerated electrons and holes, thereby enhancing the photoelectrochemical properties of the material [9]. The photocurrent density of BLT films grown on SrTiO_3 by sputtering deposition was shown to reach a value of 5.71 nA/cm² at 5 V [12].

In this study, BLT and Co-doped BLT (Co-BLT) layers were separately modified with FeCo-doped BLT (FeCo-BLT) layers to synthesize dual ferroelectric composites. These composites were produced to expand the photoresponse range, effectively suppress photogenerated carrier complexes, and improve the photoelectrochemical properties of BLT and Co-BLT. Additionally, the effect of external field polarization on the photoelectrochemical properties of the dual ferroelectric composites was investigated. The results of this study can be used to improve the photoelectrochemical and photocatalytic properties of ferroelectric composites.

2. Experiment Detail

2.1. Materials and Methods

The BLT, Co-BLT, and FeCo-BLT ceramic targets were produced by a solid-state reaction between the following powders: Bi_2O_3 (99.9%, Kojundo Chemical Co., Ltd., Sakado, Japan), TiO_2 (99.99%, Kojundo Chemical Co., Ltd., Sakado, Japan), La_2O_3 (99.99%, Kojundo Chemical Co., Ltd., Sakado, Japan), Fe_2O_3 (99.9%, Ko/741jundo Chemical Co., Ltd., Sakado, Japan), and Co_3O_4 (99.99%, Kojundo Chemical Co., Ltd., Sakado, Japan). All powders were blended thoroughly at stoichiometric ratios in a ball mill for 24 h, then dried in an oven at 100 °C and calcined in air at 700 °C for 2.5 h. The powders were then pressed for 5 min at a pressure of 50 MPa and sintered at 950 °C for 2.5 h [13].

The BLT, Co-BLT, and FeCo-BLT ceramic chemical concentrations were controlled to produce $\text{Bi}_{3.25}\text{La}_{0.75}\text{Co}_1\text{Ti}_2\text{O}_{12}$ and $\text{Bi}_{3.25}\text{La}_{0.75}\text{Fe}_{0.25}\text{Co}_{0.75}\text{Ti}_2\text{O}_{12}$. The Co-BLT and FeCo-BLT ceramic targets had pristine BLT phases, as indicated by the θ - 2θ values for their X-Ray diffraction (XRD) peaks [14]. Prior to the modification of FeCo-BLT with BLT and Co-BLT films, the fabricated BLT and Co-BLT films were deposited onto Nb:SrTiO₃ (001) (Nb-STO) substrates by a 90-degree off-axis radio frequency magnetron sputtering (Korea Vacuum Tech., Gimpo, Republic of Korea) in Ar gas at a temperature and working pressure of 750 °C and 135 m torr, respectively. The deposition time and RF power of the procedure were 1 h and 50 W, respectively. Subsequently, the FeCo-BLT films were sputtered on the previously sputtered BLT and Co-BLT films under the same conditions [15–18]. Finally, the BLT/FeCo-BLT and Co-BLT/FeCo-BLT films were deposited on the Nb-doped (0.5 wt.%) Nb-SrTiO₃ (001) substrates used as the bottom electrode. The top electrode was etched by photolithography (Nextron, Busan, Republic of Korea), and a Au top electrode (150 μm diameter) was deposited on the film using a thermal evaporator (Nano Tech Planet Co., Ltd., Bucheon, Republic of Korea) [19,20].

2.2. Characteristic Measurements

The crystal structures and phase identification of the powders of the sintered pellets were determined with an X-Ray diffractometer (Rigaku, Tokyo, Japan, D/MAX 2200) using Cu-K α radiation ($\lambda = 1.5418$ Å) with an angular step of 0.02 /min. The microstructures of the pelletized powders were examined using scanning electron microscopy (SEM, Hitachi, S-4700, Hitachi, Japan) and atomic force microscopy (AFM) (Park NX10, Park Systems, Chiyoda City, Tokyo), and the dielectric measurements were performed using an Agilent

4263 B LCR meter (Agilent, Santa Clara, CA, USA). The dielectric permittivity was acquired in the frequency of 100 kHz as a function of temperature (T) across a temperature range of 25–700 °C. The optical properties were analyzed using a 100 W solar simulator (K3000, McScience, Gyeonggi-do, Republic of Korea). The photocurrent density of the film was measured between the Au electrodes (45 μm space) after putting each tip in contact with its respective electrode.

3. Results and Discussions

The epitaxial crystalline quality of the grown films was determined with X-Ray diffraction (XRD) ($\lambda = 1.5405 \text{ \AA}$) using a Cu-K α source. Figure 1 shows the theta-2 θ scans of BLT/FeCo-BLT and Co-BLT/FeCo-BLT films grown on (001) oriented Nb-SrTiO₃ substrates. The XRD patterns show that all the films were grown on 001 orientation, and the BLT crystal structures of BLT/FeCo-BLT and Co-BLT/FeCo-BLT films were maintained. This indicates that the modification of FeCo-BLT films does not lead to the formation of other phases of BLT and Co-BLT. The diffraction peaks of the special samples, appearing at $2\theta = 21.74^\circ$, $2\theta = 44.27^\circ$, etc., are consistent with the crystallographic positions of BLT (008) and (0016), respectively. The wigggle curve of the (0016) reflection was measured to determine the out-of-plane mosaic diffusion and crystalline quality. This indicates the good crystallinity of the prepared BLT/FeCo-BLT and Co-BLT/FeCo-BLT composite films.

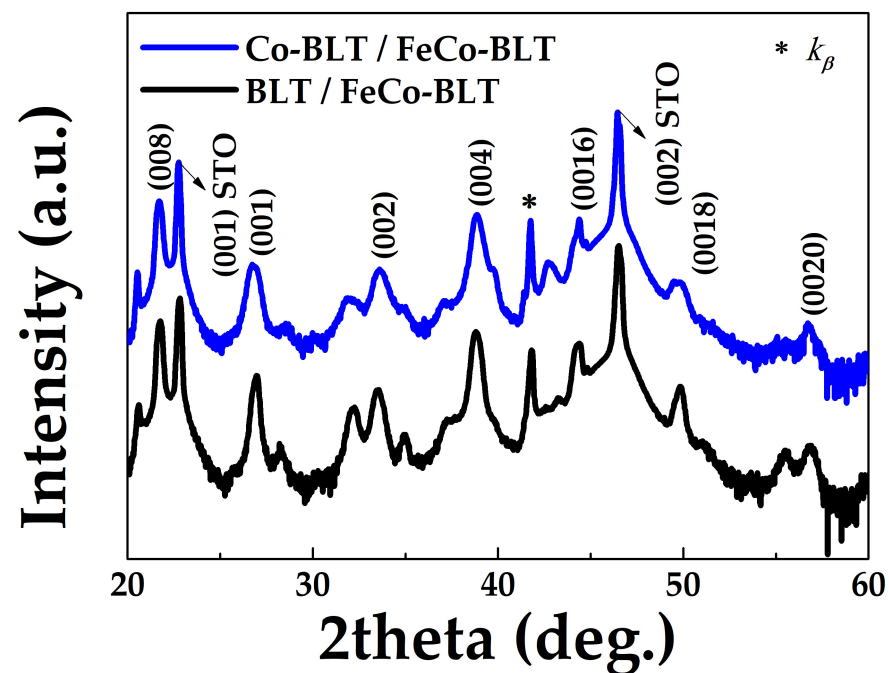


Figure 1. The X-Ray θ - 2θ diffraction patterns for BLT/FeCo-BLT (BLFCT), and Co-BLT (BLCT)/FeCo-BLT (BLFCT) epitaxial films on Nb-SrTiO₃ (Nb-STO) (001).

The surface morphologies of the grown BLT/FeCo-BLT and Co-BLT/FeCo-BLT samples were compared using SEM and atomic force microscopy (AFM) (Figure 2). In Figure 2a, the nanostructure of the CoFe₂O₄ phases on the surface of the film is square and uniformly distributed, similar to our previous result [21] that used the pulsed laser deposition method. Based on the morphology observation, the chemical contents are similar to our previous report [21]. The nanoparticles on the surface of the film were large squares, 0.6 nm in size, and six-fold larger than that of the BLT case (Figure 2b). This may be due to the difference between the base layers of BLT and Co-BLT in the bilayer ferroelectric films. BLT/FeCo-BLT contained more Co-ions than Co-BLT/FeCo-BLT, and excess ions cannot be replaced by large particles on the surface. AFM measurements were performed at multiple locations across the sample, as shown in Figure 2c,d. This was conducted to assess

the stability and large-area uniformity of the BLT/FeCo-BLT and Co-BLT/FeCo-BLT thin films on Nb-STO and to elucidate the architecture of the resulting structures and determine their size. In particular, the root mean square roughness of the stripes was 4.9 and 9.1 nm for the BLT/FeCo-BLT and Co-BLT/FeCo-BLT films, respectively, indicating that they have smooth, dense, and crack-free surface morphologies.

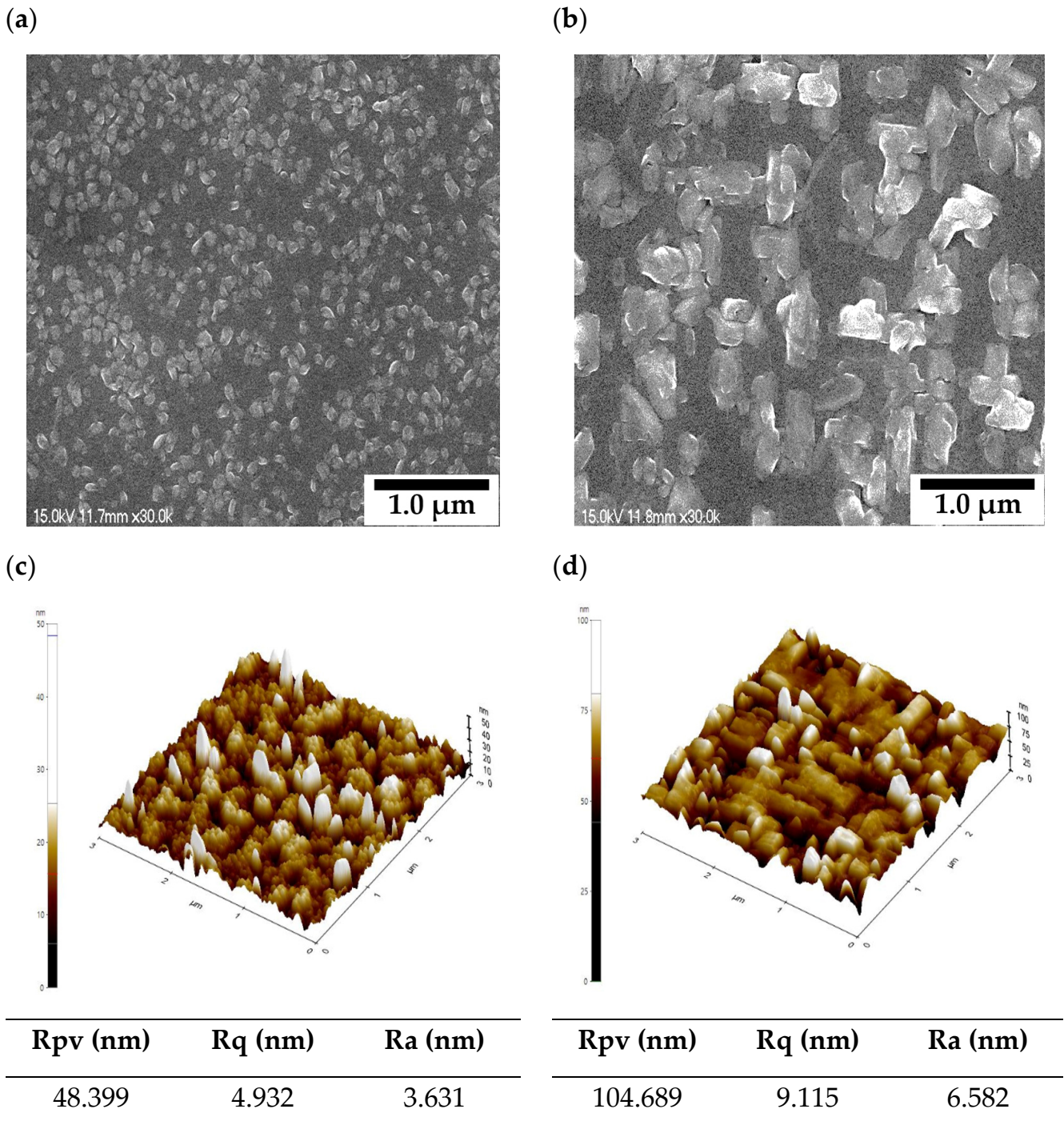


Figure 2. (a,b) SEM and (c,d) AFM results of BLT/FeCo-BLT (BLFCT) and Co-BLT (BLCT)/FeCo-BLT (BLFCT) surface morphologies on Nb-SrTiO₃ (STO) substrate.

Figure 3 shows the dielectric constants and temperature dependencies of the BLT/FeCo-BLT and Co-BLT/FeCo-BLT composite films at a frequency of 10 kHz. The dielectric constants of the samples gradually increased as the FeCo-BLT films

were modified. The peak temperature of the dielectric spectrum corresponded to the ferroelectric–paraelectric phase transition temperature, i.e., the Curie temperature (T_c), as shown in the interpolation of Figure 4. The Curie temperatures of the pure BLT, Co–BLT, and FeCo–BLT ceramics were 400, 500, and 600 °C, respectively, at a frequency of 10 kHz; the T_c of pure BLT corresponded to that of pure BLT in previous studies [22,23]. The BLT/FeCo–BLT and Co–BLT/FeCo–BLT composite films had ferroelectric temperatures of 650 °C and 700 °C, respectively, which were significantly higher than that of the base target. These high ferroelectric properties were maintained until 650 °C, indicating that the modification of the BLT and Co–BLT films with FeCo–BLT improved the thermal stability of the ferroelectric properties of the films [24–27]. The BLT/FeCo–BLT and Co–BLT/FeCo–BLT composite films exhibited favorable ferroelectric properties and thermal stability.

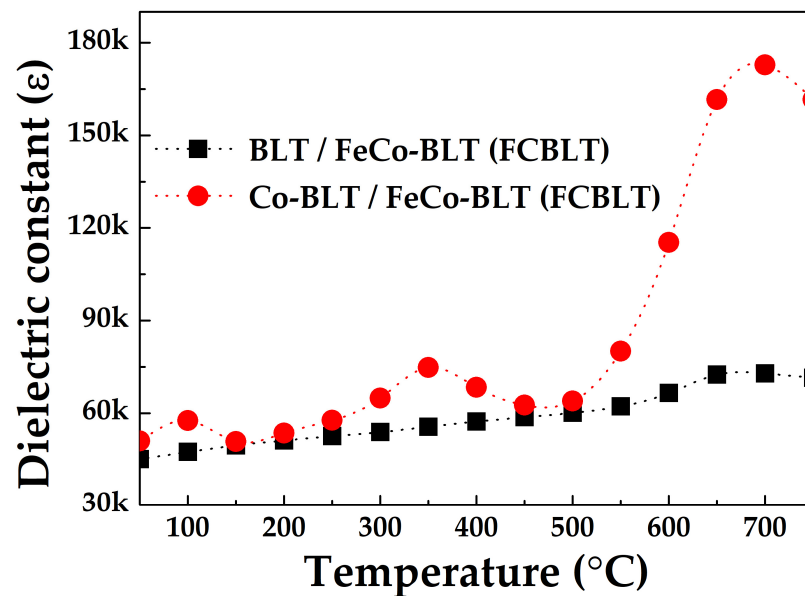


Figure 3. Dielectric constant at 10 kHz as a function of temperature for BLT/FeCo–BLT (BLFCT), and Co–BLT (BLCT)/FeCo–BLT (BLFCT) film on Nb-STO. The inset image is the dielectric constant at 10 kHz as a function of temperature for BLT, BLCT, and BLFCT bulk.

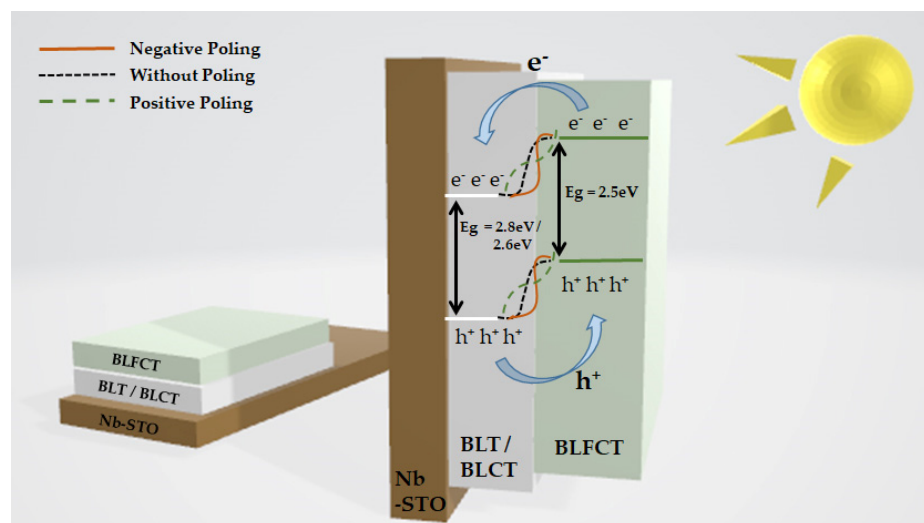


Figure 4. Schematic diagram of BLT/FeCo–BLT (BLFCT), and Co–BLT (BLCT)/FeCo–BLT (BLFCT) film band energy on Nb-STO substrate.

Figure 4 shows a schematic of the heterojunction energy-level structures of the BLT/FeCo-BLT and Co-BLT/FeCo-BLT composite films. Illumination excited the photo-generated electrons in the valence band of the BLT/FeCo-BLT and Co-BLT/FeCo-BLT composites to their respective conduction bands; however, the high position of the FeCo-BLT conduction band resulted in the excitation of its photogenerated electrons to the conduction bands of BLT and Co-BLT upon illumination. Owing to the lower valence band positions of BLT and Co-BLT, the photogenerated holes in the valence bands of these composites were transferred to the valence band of FeCo-BLT; thereby, the photogenerated electrons and holes were separated effectively, prolonging the lifetime of the photogenerated carriers [28,29]. Because BLT and FeCo-BLT are ferroelectric materials, their internal spontaneous polarizations and external field polarizations change the degree of energy band bending at the interface and affect the transfer of photogenerated charge [30–33]. After positive external field polarization, both the downward bending of the FeCo-BLT energy band at the interface of BLT and Co-BLT as well as the upward bending of Co-BLT with the increased FeCo-BLT energy band results in an increase in the width of the depletion layer. This facilitated the transport of photogenerated carriers and enhanced the photoelectrochemical performance of the composite. After negative external field polarization, the depletion layer width decreased, and the energy band bending at the interfaces of BLT and FeCo-BLT decreased, hindering the transport of photogenerated carriers [34].

The photovoltaic responses of the BLT/FeCo-BLT and Co-BLT/FeCo-BLT composite films deposited on Nb:SrTiO₃ substrates were measured under 100 W solar simulator irradiation, as shown in Figure 5a,b. The measurements were performed at room temperature, and the ferroelectric films were not subjected to polarization treatment. The FeCo-BLT-modified BLT and Co-BLT composite films had an open-circuit voltage of 4 V and corresponding short-circuit photocurrent densities of 155.4 and 424.66 $\mu\text{A}/\text{cm}^2$, respectively [35,36].

Modifying the BLT and Co-BLT films with the FeCo-BLT film resulted in composites with stronger photovoltaic properties and higher short-circuit currents than their predecessors. The differences in photovoltaic performances between the BLT/FeCo-BLT and Co-BLT/FeCo-BLT composite films were owed to their self-polarization phenomena and not to their similar crystal structures and optical bandgaps.

The photocurrent of BLT/FeCo-BLT and Co-BLT/FeCo-BLT composite films had the same direction as the depolarization field, indicating that this field propelled the separation of photogenerated electron-hole pairs and that the upward self-polarization determined the photovoltaic performance. This was consistent with FeCo-BLT modification as the composite films had the largest ratio of upward self-polarization. Owing to the modification of the FeCo-BLT films, the conductivity mechanism of the BLT/FeCo-BLT and Co-BLT/FeCo-BLT composite films changed from an interfacial Schottky emission model to a space-charge limited current, and the built-in electric field at the interface was weakened to promote the separation of photogenerated electron-hole pairs under the effect of the depolarization field.

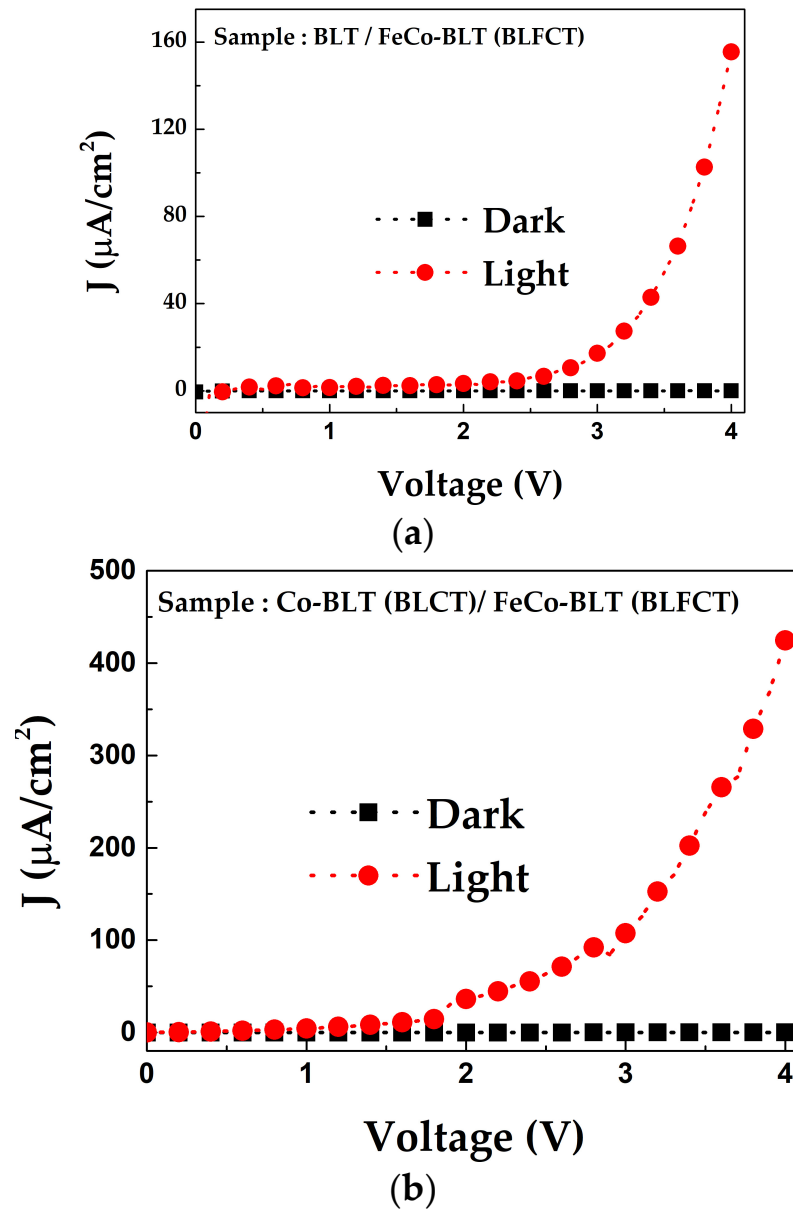


Figure 5. Photovoltaic responses of the BLT/FeCo-BLT (BLFCT), and Co-BLT (BLCT)/FeCo-BLT (BLFCT) film. (a) The photocurrent density (J) of the BLT/BLFCT films on Nb-STO. (b) The photocurrent density (J) of the BLCT/BLFCT films on Nb-STO substrate.

4. Conclusions

In this study, BLT/FeCo-BLT and Co-BLT/FeCo-BLT bilayer ferroelectric films were deposited on Nb-STO substrates by RF sputtering. The effect of the FeCo-BLT films on the electrical and optoelectronic properties of BLT and Co-BLT, as well as on their microstructures, was investigated. The external field polarization treatment of the ferroelectric materials led to the bending of the energy band and subsequent acceleration of the photo-generated charge transfer. This resulted in BLT/FeCo-BLT and Co-BLT/FeCo-BLT bilayer ferroelectric films with large photoresponsive current densities and a maximum photocurrent density of $424.66 \mu\text{A}/\text{cm}^2$. The modification of BLT and Co-BLT by FeCo-BLT maintained the ferroelectric properties below 650°C , while the bandgap value decreased to approximately 2 eV. We can infer that this method can reduce the bandgap while improving photovoltaic power generation performance. These results improve our understanding of the potential of ferroelectric thin films in photovoltaic power generation.

Author Contributions: Sample fabrication and original draft preparation, R.T. and R.H.; supervision and editing, S.K. and C.W.B. All authors have read and agreed to the published version of the manuscript.

Funding: Creative Materials Discovery Program (2017M3D1A1040828), the Korea Basic Institute grant funded by the Ministry of Education (2020R1A6C103A050), and the Gachon University research fund of 2019 (GCU-2019-0800).

Institutional Review Board Statement: Not applicable.

Informed Consent Statement: Not applicable.

Data Availability Statement: Not applicable.

Conflicts of Interest: The authors declare no conflict of interest.

References

1. Zhang, Y.; Jie, W.; Chen, P.; Liu, W.; Hao, J. Ferroelectric and piezoelectric effects on the optical process in advanced materials and devices. *Adv. Mater.* **2018**, *30*, e1707007. [[CrossRef](#)] [[PubMed](#)]
2. Frisenda, R.; Molina-Mendoza, A.J.; Mueller, T.; Castellanos-Gomez, A.; van der Zant, H.S.J. Atomically thin p–n junctions based on two-dimensional materials. *Chem. Soc. Rev.* **2018**, *47*, 3339–3358. [[CrossRef](#)] [[PubMed](#)]
3. Sharma, K.; Sharma, V.; Sharma, S.S. Dye-sensitized solar cells: Fundamentals and current STATUS. *Nanoscale Res. Lett.* **2018**, *13*, 381. [[CrossRef](#)] [[PubMed](#)]
4. Huang, H. Ferroelectric photovoltaics. *Nat. Photonics* **2010**, *4*, 134–135. [[CrossRef](#)]
5. Tan, L.Z.; Zheng, F.; Young, S.M.; Wang, F.; Liu, S.; Rappe, A.M. Shift current bulk photovoltaic effect in polar materials—Hybrid and oxide perovskites and beyond. *npj Comput. Mater.* **2016**, *2*, 16026. [[CrossRef](#)]
6. Lopez-Varo, P.; Bertoluzzi, L.; Bisquert, J.; Alexe, M.; Coll, M.; Huang, J.; Jimenez-Tejada, J.A.; Kirchartz, T.; Nechache, R.; Rosei, F.; et al. Physical aspects of ferroelectric semiconductors for photovoltaic solar energy conversion. *Phys. Rep.* **2016**, *653*, 1–40. [[CrossRef](#)]
7. Tataroğlu, A.; Al-Ghamdi, A.; Yakuphanoglu, F. Frequency dependence of dielectric parameters of structure with Bi₃. 25La₀.75Ti₃O₁₂ thin film prepared by sol-gel method. *J. Optoelectron. Adv. Mater.* **2017**, *19*, 629–633.
8. Silva, J.P.B.; Silva, J.M.B.; Oliveira, M.; Weingärtne, T.; Sekhar, K.C.; Pereira, M.; Gomes, M.J.M. High-Performance Ferroelectric–Dielectric Multilayered Thin Films for Energy Storage Capacitors. *Adv. Funct. Mater.* **2019**, *29*, 1807196. [[CrossRef](#)]
9. Wang, K.; Wu, C.; Hou, Y.; Yang, D.; Priya, S. Monocrystalline perovskite wafers/thin films for photovoltaic and transistor applications. *J. Mater. Chem. A* **2019**, *7*, 24661–24690. [[CrossRef](#)]
10. Huang, Y.-T.; Kavanagh, S.R.; Scanlon, D.O.; Walsh, A.; Hoyer, R.L. Perovskite-inspired materials for photovoltaics and beyond—From design to devices. *Nanotechnology* **2021**, *32*, 132004. [[CrossRef](#)]
11. Butler, K.T.; Frost, J.M.; Walsh, A. Ferroelectric materials for solar energy conversion: Photoferroics revisited. *Energy Environ. Sci.* **2014**, *8*, 838–848. [[CrossRef](#)]
12. An, H.; Han, J.Y.; Kim, B.; Song, J.; Jeong, S.Y.; Franchini, C.; Bark, C.W.; Lee, S. Large enhancement of the photovoltaic effect in ferroelectric complex oxides through bandgap reduction. *Sci. Rep.* **2016**, *6*, 28313. [[CrossRef](#)]
13. He, R.; Kim, S.M.; Kim, M.R.; Tang, R.; Bark, C.W. Preparation of Hexagonal SrMnO₃ High-Quality Target for Magnetron Sputtering. *J. Nanosci. Nanotechnol.* **2021**, *21*, 4005–4010. [[CrossRef](#)]
14. Choi, W.S.; Chisholm, M.F.; Singh, D.J.; Choi, T.; Jellison, G.E., Jr.; Lee, H.N. Wide bandgap tunability in complex transition metal oxides by site-specific substitution. *Nat. Commun.* **2021**, *3*, 689. [[CrossRef](#)]
15. He, R.; Kim, M.R.; Tang, R.; Kim, S.; Bark, C.W. Epitaxial Growth of SrMnO₃ Films on SrTiO₃ Substrates by Off-Axis Angle Radio Frequency Magnetron Sputtering. *Sci. Adv. Mater.* **2021**, *13*, 1344–1349. [[CrossRef](#)]
16. Tang, R.; Kim, S.; Bark, C.W. Change of Phase Transition Temperature in Band Engineered Ferroelectric Lanthanum-Modified Bismuth Titanates. *J. Nanosci. Nanotechnol.* **2020**, *20*, 7135–7139. [[CrossRef](#)]
17. Tang, R.; He, R.; Kim, S.; Bark, C.W. Ferroelectric B-Site Modified Bismuth Lanthanum Titanate Thin Films for High-Efficiency PV Systems. *Coatings* **2022**, *12*, 1315. [[CrossRef](#)]
18. Yue, W.; Yu, L.; Liu, L.; Cai, Y.; Li, T.; Jia, T.; Yu, S.; Sun, R. SrTiO₃-Bi₃.25La₀.75Ti₃O₁₂ energy storage film capacitors fabricated on silicon-based substrates. In Proceedings of the 23rd International Conference on Electronic Packaging Technology (ICEPT), Dalian, China, 10–13 August 2022; pp. 1–5. [[CrossRef](#)]
19. An, H.; Choi, Y.-G.; Jo, Y.-R.; Hong, H.J.; Kim, J.-K.; Kwon, O.; Kim, S.; Son, M.; Yang, J.; Park, J.-C.; et al. Experimental realization of strain-induced room-temperature ferroelectricity in SrMnO₃ films via selective oxygen annealing. *NPG Asia Mater.* **2021**, *13*, 1–10. [[CrossRef](#)]
20. Lee, S.K.; Bark, C.W. Crystallographic structure and ferroelectricity of epitaxial hafnium oxide thin films. *J. Korean Ceram. Soc.* **2021**, *59*, 25–43. [[CrossRef](#)]
21. An, H.; Hong, H.J.; Jo, Y.-R.; Jung, S.-G.; Kim, S.; Kim, S.; Lee, J.; Choi, H.; Yoon, H.; Kim, S.-Y.; et al. Reversible magnetoelectric switching in multiferroic three-dimensional nanocup heterostructure films. *NPG Asia Mater.* **2019**, *11*, 68. [[CrossRef](#)]

22. Rachna, S.; Gupta, S.M.; Bhattacharyya, S. Impedance analysis of Bi_{3.25}La_{0.75}Ti₃O₁₂ ferroelectric ceramic. *Pramana* **2008**, *71*, 599–610. [[CrossRef](#)]
23. Pak, J.; Nam, K.; Lee, J.; Park, G. Fabrications and electrical properties of ferroelectric Bi_{3.25}La_{0.75}Ti₃O₁₂ thin films using an indium–tin-oxide conductive layer as the bottom electrode. *J. Phys. Condens. Matter* **2004**, *16*, 4983. [[CrossRef](#)]
24. Kim, S.; Nguyen, T.M.H.; He, R.; Bark, C.W. Particle size effect of lanthanum-modified bismuth titanate ceramics on ferroelectric effect for energy harvesting. *Nanoscale Res. Lett.* **2021**, *16*, 115. [[CrossRef](#)] [[PubMed](#)]
25. Ma, S.; Li, W.; Hao, J.; Ren, S.; Wang, M.; Xu, Z. Microstructure and ferroelectric properties of Ta-doped Bi_{3.25}La_{0.75}Ti₃O₁₂/ZnO thin film capacitors. *Ceram. Int.* **2021**, *48*, 5239–5245. [[CrossRef](#)]
26. Kim, M.; Kim, S.; Roh, J.G.; Kim, Y.; Bark, C.W. Properties of the mesoporous perovskite solar cell by plasma surface activation with a titanium dioxide electrode. *Mol. Cryst. Liq. Cryst.* **2021**, *735*, 84–92. [[CrossRef](#)]
27. An, H.; Kim, J.-K.; Jung, S.-G.; Kim, S.; Na, K.; Yang, J.; Song, J.; Park, T.; Bark, C.W.; Kim, S.; et al. Tunable Magnetism and Morphology of Ferromagnetic Nanocups in Perovskite Ferroelectric Films via Co Exsolution of Transition Metals. *ACS Appl. Electron. Mater.* **2022**, *4*, 4499–4506. [[CrossRef](#)]
28. Kim, M.R.; Kim, S.M.; Bark, C.W. Characterization of perovskite solar cells with a solution-processed two-stage SnO₂ electron transport layer. *Mol. Cryst. Liq. Cryst.* **2021**, *735*, 75–83. [[CrossRef](#)]
29. Oh, I.-K.; Zeng, L.; Kim, J.-E.; Park, J.-S.; Kim, K.; Lee, H.; Seo, S.; Khan, M.R.; Kim, S.; Park, C.W.; et al. Surface energy change of atomic-scale metal oxide thin films by phase transformation. *ACS Nano* **2020**, *14*, 676–687. [[CrossRef](#)]
30. Zhang, Y.; Gu, R.; Zheng, S.; Liao, K.; Shi, P.; Fan, J.; Xu, Q.; Min, Y. Long-life Li–S batteries based on enabling the immobilization and catalytic conversion of polysulfides. *J. Mater. Chem. A* **2019**, *7*, 21747–21758. [[CrossRef](#)]
31. Song, J.; Kim, T.L.; Lee, J.; Cho, S.Y.; Cha, J.; Jeong, S.Y.; An, H.; Kim, W.S.; Jung, Y.-S.; Park, J.; et al. Domain-engineered BiFeO₃ thin-film photoanodes for highly enhanced ferroelectric solar water splitting. *Nano Res.* **2017**, *11*, 642–655. [[CrossRef](#)]
32. Shi, J.; Zhao, P.; Wang, X. Piezoelectric-polarization-enhanced photovoltaic performance in depleted-heterojunction quantum-dot solar cells. *Adv. Mater.* **2012**, *25*, 916–921. [[CrossRef](#)]
33. Jeong, S.Y.; Song, J.; Lee, S. Photoelectrochemical device designs toward practical solar water splitting: A review on the recent progress of BiVO₄ and BiFeO₃ photoanodes. *Appl. Sci.* **2018**, *8*, 1388. [[CrossRef](#)]
34. Xie, J.; Guo, C.; Yang, P.; Wang, X.; Liu, D.; Li, C.M. Bi-functional ferroelectric BiFeO₃ passivated BiVO₄ photoanode for efficient and stable solar water oxidation. *Nano Energy* **2017**, *31*, 28–36. [[CrossRef](#)]
35. Nguyen, T.M.H.; Bark, C.W. In-Situ Piezoelectric Effect for Augmenting Performance of Self-Powered ZnO-Based Photo-detector. *Coatings* **2023**, *13*, 921. [[CrossRef](#)]
36. Nguyen, T.M.H.; Garner, S.M.; Bark, C.W. Metal Electrode-Free Halide Perovskite-Based Flexible Ultraviolet-C Photodetector with Large Area. *Nanoscale Res. Lett.* **2022**, *17*, 94. [[CrossRef](#)]

Disclaimer/Publisher’s Note: The statements, opinions and data contained in all publications are solely those of the individual author(s) and contributor(s) and not of MDPI and/or the editor(s). MDPI and/or the editor(s) disclaim responsibility for any injury to people or property resulting from any ideas, methods, instructions or products referred to in the content.